Effect of substrate temperature on structural and materials properties of zirconium nitride films on D9 steel substrates

K. Ashok[1], B. Subramanian*[1], P. Kuppusami[2], and M. Jayachandran[1]

[1] ECMS division, Central Electrochemical Research Institute, Karaikudi-630 006, India
[2] Physical Metallurgy Section, Indira Gandhi Centre for Atomic research, Kalpakkam-603102, India

Thin zirconium nitride (ZrN) films were prepared by using reactive direct current (DC) magnetron sputtering onto D9 steel substrates. XRD technique was employed to study the coatings, observing variations of crystallite size, crystallite texture and lattice constant, as a function of substrate temperature. Chemical states of the ZrN thin films were determined by X-ray photoelectron microscopy (XPS). AFM picture showed the presence of spherical shaped grains on the top of homogeneous granular surface. The hardness and elastic modulus values were measured by nanoindendation and their values are 18.5 and 343 GPa respectively.

1 Introduction

Zirconium nitride (ZrN) is a compound of the period V in group V-B which exhibits suitable properties for a great variety of industrial applications [1,2]. Stoichiometric ZrN compound is the only stable phase with a gold-like colour due to its metallic band structure. Other non-stoichiometric metastable phase also exists like Zr_2N, ZrN_2, Zr_3N_4 and Zr_4N_3 [3]. These films are used as wear resistant coating on steel drill bits, as diffusion barrier in IC technology, as cryogenic thermometer, as hard coatings, as a protective coating on D9 steel vessels handling molten metal and as solar energy collector surface film, Josephson junctions [4-8]. These coatings appear to have substantial potential in aero engine, industrial and biological application [9]. ZrN thin films have been synthesized by chemical vapor deposition, pulsed laser deposition [10], ion-beam assisted deposition [11], reactive sputtering [12], plasma nitridation [13], vacuum arc deposition [14], ion plating [15], cathodic arc evaporation [16], and ultra high vacuum sputtering [17].

More recently, ZrN began to be used as protective and decorative coating, mostly due to its better corrosion resistance than TiN, the present commercial counterpart. Since ZrN has a higher negative free energy of formation than TiN, ZrN seemed to form itself more easily than TiN [18]. The microstructure and properties of ZrN film would vary with different deposition techniques and processing parameters [19]. Substrate temperature (Ts) has a strong influence on structural and morphological characteristics of the films, because they are correlated with the thermal energy employed to condense the material on the substrate surface [20].

The micro hardness of the coating is found to depend strongly on structural parameters such as crystallographic orientation, micro strain, and crystallite size. The physical properties of thin films are often anisotropic and controlled by their detailed microstructure, including atomic ratio (stoichiometry), crystallinity and preferred-orientation, which are complex functions of the growth parameters for a given growth method.

Here, in this paper, we have investigated the dependence of the phase, texture and microstructure of ZrN on varying the substrate temperature during film growth by reactive dc magnetron sputtering and optimized the

* Corresponding author: e-mail: subramanianb3@gmail.com

substrate temperature. The materials properties of the ZrN film prepared at the optimized parameters are discussed in this paper.

2   Experimental

ZrN thin films of 2 μm thickness were deposited on D9 steel (Composition is given in table 1) substrate using a 12" HINDHIVAC DC magnetron sputter deposition unit. The base vacuum of the chamber was below 1x 10^{-6} Torr at different substrate temperatures. High purity argon was fed into the vacuum chamber for the plasma generation. The deposition parameters for ZrN sputtering are summarized in table 2.

Table 1   Composition of D9 stainless steel used in the present study.

Element	Ni	Cr	Mn	Mo	Ti	Nb	Si	C	Fe
Wt.%	14.7	15	1.5	2.2	0.3	0.167	0.67	0.05	Bal.

Table 2   Deposition parameters of ZrN thin film.

| Objects	Specification
Target	Zr (99.9 %)
Substrate	D9 steel
Target to substrate distance	60 mm
Ultimate vacuum	1 x 10^{-6} m bar
Operating vacuum	2 x 10^{-3} m bar
Sputtering gas (Ar: N_2)	60:40
Power	180 Watt
Substrate temperature	100°C, 200 °C, 300°C

The crystal structure and preferred orientation of the ZrN coatings were examined by XRD using PANalytical - 3040 X'pert pro diffractometer operated at 40KV and 30 mA with Cu K_α (1.5414 Å) radiation with 0.02° step size. The value of texture coefficient, (T_c), was calculated using the equation:

$$T_c = \frac{I_m(hkl)/I_o(hkl)}{\frac{1}{n}\sum_{1}^{n} I_m(hkl)/I_o(hkl)} \, , \tag{1}$$

where $I_m(hkl)$ is the reflected intensity from hkl crystallographic planes in the textured specimen, and $I_o(hkl)$ is the standard intensity, and n is the total number of reflections measured. The T_c value for a particular set of planes (hkl) is proportional to the number of grains that are oriented with this plane parallel to the surface of the specimen. The surface of the coatings was analyzed using a Molecular Imaging Atomic force microscope. The chemical nature of the outermost part of ZrN film was obtained by X-ray photoelectron spectroscopy (XPS) using Multilab 2000. A Renishaw Ramascope System 2000 spectrometer was used for Laser Raman experiments. The microscope attachment was an Olympus BH2 system. Power of 2–3 mW was incident on the samples in a 2 μm diameter spot through a standard ×50 microscope objective. The spectra were collected with a 200 s data point acquisition time, a spectral range of 100–1500 cm^{-1} and a spectral resolution of 3–4 cm^{-1}. Spectra are presented as intensity (counts) versus Raman shift (cm^{-1}). The nano mechanical tests were investigated by means of a nanoindenter (NHTX S/N: 50-0172). For the nanohardness and elastic modulus measurement, the nanoindenter was equipped with a Berkovich diamond probe tip, 3-sided pyramidal indenter. The tip radius is around 100 nm. The loading and unloading rates of the nanoindentation were 10 mN/min. The holding time was 5 s for each indent. The nano hardness and elastic modulus of each indent was determined on the basis of Oliver and Pharr method.

3   Results and discussion

X-ray diffraction patterns of ZrN thin films grown at different substrate temperatures on D9 Steel (T_s= 100 °C, 200 °C, 300 °C) are shown in figure 1. Peaks corresponding to (111) and (200) planes were observed at 33.8° and 39.3° respectively for Zirconium nitride (ZrN) which matches with JCPDS file no: 02-0956 and the peak obtained at 61.9° corresponds to (222) plane of Zirconium nitride (Zr_3N_4) phase. When the T_s increases, the intensity of the plane (111) decreases and (200) increases. At the substrate temperature of 200 °C, the intensity of the (200) plane is greater than the (111) peak as indicated in figure 1. The researchers suggest that the preferential orientation is determined by the competition between two thermodynamic parameters, the free surface energy and the strain energy.
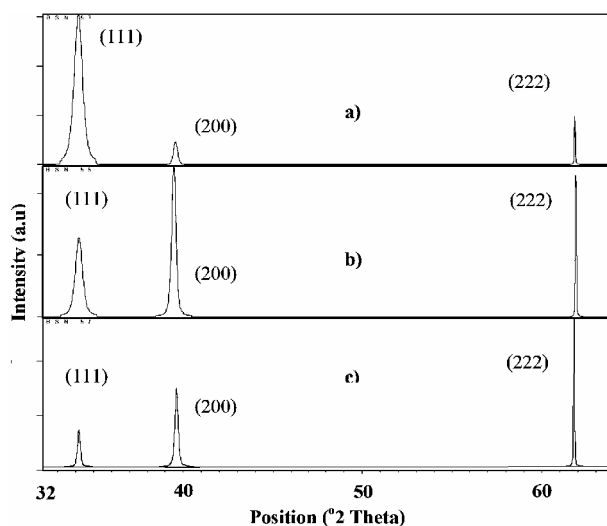
Fig. 1 X-ray diffraction pattern of Zirconium nitride thin film at different substrate temperatures a) 100 °C b) 200 °C and c) 300 °C.
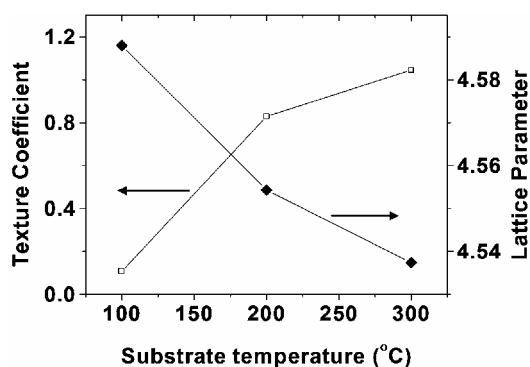
Fig. 2 Variation of texture coefficient and lattice parameter with the substrate temperatures. The e.s.d for T_c and lattice parameter was 0.1 and 0.01 respectively.

The calculated crystallite size values obtained from Debye – scherrer formula are 13.2, 20.4 and 15.5 nm for the films deposited at different substrate temperatures 100 °C, 200 °C and 300 °C respectively. When T_s is very low, the ad atoms have low mobility and the grouping for the nucleation and the formation of islands is difficult, producing individual and isolated small grain sizes [21]. When Ts is increased, the mobility of ad atoms also increases, favoring the grouping and the nucleation, producing an increase in the grain size. But there is a limit in this process. At very high temperature, the ad atoms are desorbed which could be because of the greater absorption energy than the surface energy [22]. The maximum value of grain size of the film grown at 200 °C is also an evidence of its high compaction (decreasing the grain boundaries), confirmed by the higher intensity of the diffraction peak at this temperature.

The fact that the lattice parameter is lower than the one for the material in bulk (4.61Å) means that the lattice has many vacancies of nitrogen. Moreover it is observed that this parameter decreases as a function of T_s, which means that these vacancies increase with temperature because the re-sputtering process affects the N atoms than the Zr atoms because they are lighter.

The AFM pictures of the Zirconium Nitride (ZrN) thin films grown at different substrate temperatures are shown in figure 3 in 3D and 2D (Inset) views. The top view of the 3D pictures recorded in area of 5 μm x 5 μm show the presence of spherical granular on the top of homogeneous granular surface. The pictures clearly indicate how the shape of the top of the grain surface changes with the increase of temperature. The grains grow in blurred hill shapes at lower temperatures and obtain nice spherical shapes while increasing temperature up to 200 °C. The plane view of 2D pictures recorded in the area of 5 μm x 5 μm also reveals the formation of cluster of crystallites and improvement in grain size with growth temperature.
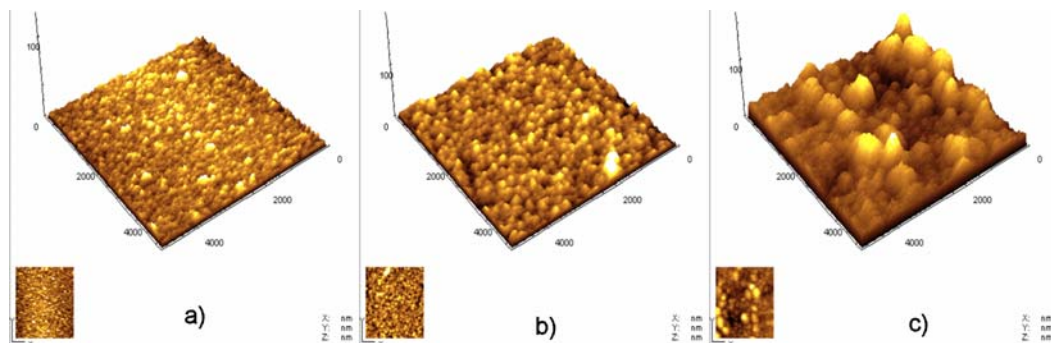
Fig. 3 AFM photographs of Zirconium Nitride thin films at different substrate temperatures a) 100 °C, b) 200 °C and c) 300 °C. (Online color at www.crt-jouranl.org)
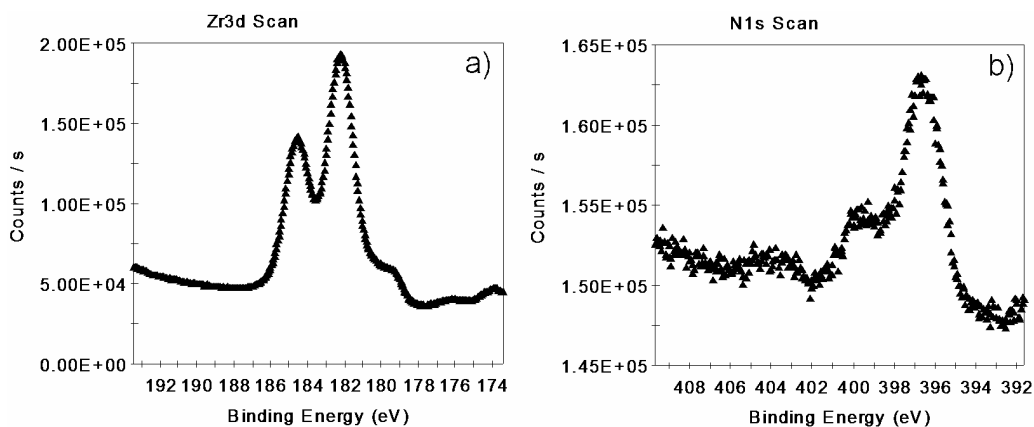

Fig. 4 X-ray Photo electron spectroscopy spectra of (a) Zr 3d and (b) N1s.

As the substrate temperature increases the grain size increases, which in turn reduces the dislocation density. The surface topography is composed of clusters of varying sizes. The irregular size of grains suggests that at low substrate temperatures, the kinetic energy is not sufficient for the coalescence of the grains. It is evident from the AFM micrographs that the shape of the grains does not change with increasing substrate temperature. The temperature dependence of growth and morphology can be explained on the basis of species on the substrate surface as follows. The evaporated atomic or molecular species on the substrate surface acquire a large thermal energy and hence a large mobility when deposited at higher substrate temperatures. This enhances the diffusion distance of the evaporated species. As a result, the collision process initiates the nucleation and enhances the island formation in order to grow continuous film with larger grains.

XPS analysis was conducted to further investigate the chemical bonding of the ZrN films. There appear two peaks on the Zr (3d) XPS spectrum, as shown in figure 4a. They are located at 182.15 and 184.35 eV, representing the binding energies of $Zr(3d_{5/2})$ and $Zr(3d_{3/2})$ electrons, respectively. But compared with the binding energy of the simple substance $Zr(3d_{5/2})$, 178.7 eV, there exist chemical shifts for both peaks, indicating that the Zr atoms are in compound states [23]. Interestingly, on the N (1s) XPS spectrum shown in figure 4b, there are correspondingly two peaks at 396.7 eV and 399.8 eV, respectively. These results suggest that ZrN have been formed during deposition.

The coatings were characterized using Raman microscopy to elucidate the behavior of the optic and acoustic phonon modes of the face centered cubic crystalline lattices. The Raman spectra of ZrN coatings deposited at the optimized substrate temperature of 200 °C as shown in figure 5. consists of two broad bands centered at 222 cm^{-1} (FWHM= 130 cm^{-1}) in the acoustic region which is done to the vibrations of the heavy Zr ions and in the optic region at 511 cm^{-1} (FWHM= 230 cm^{-1}) which is due to the vibrations of the lighter N ions. This is in good agreement with the reported Raman studies for ZrN films reported by Constable et al. [24]. The

asymmetry (~ 500 cm^{-1}), of the bands is due to the superposed contributions of disorder of optical phonons and second order combination of acoustic and optical processes [25].
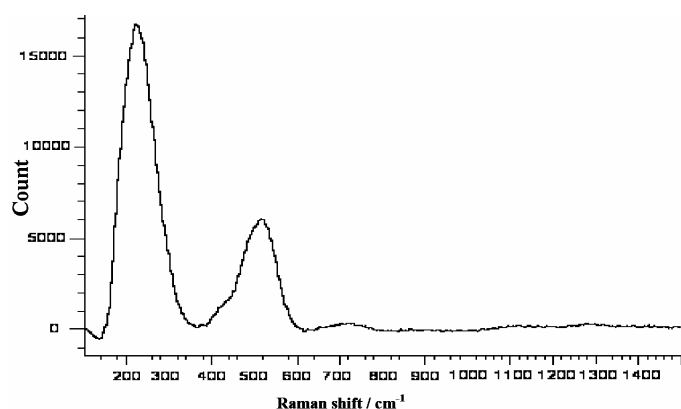
Fig. 5 Laser Raman spectra obtained for the sputtered ZrN thin film deposited at substrate temperature of 200 °C.
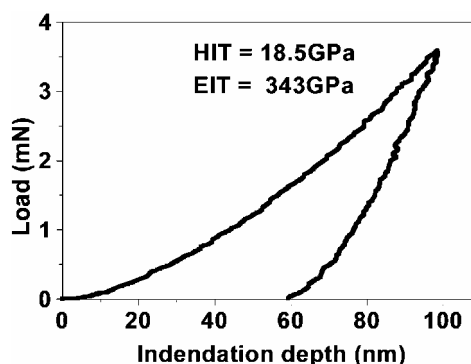
Fig. 6 Load – Indentation depth for Zirconium nitride thin film deposited at substrate temperature of 200 °C.

Nanoindentation provides a method of near surface measurements to reduce substrate effect because the direct observation of the contact impression size is not necessary. Figure 6 displays a typical load-displacement curve from which the hardness can be evaluated from the following equation [26] H= P_{Max}/ A, where P_{Max} is the maximum load, and A is the projected area determined from the function of depth. Upon unloading, the elastic displacements were recovered and the plastic displacements were retained. The indentation depth was lower than 100 nm, which in turn was less than 10% of the film thickness used. The nanohardness and the Young's modulus of the ZrN thin film prepared at the optimized T_s of 200 °C were 18.5 GPa and 343 GPa respectively. The higher value of hardness could be because of the presence of strained domains [27].

4   Conclusions

Zirconium nitride (ZrN) thin films were successfully prepared by using reactive direct current (DC) magnetron sputtering onto D9 steel substrates. At the substrate temperature of 200 °C, the intensity of the (200) plane was greater than the (111) peak. The maximum value of grain size of the film grown at 200 °C was confirmed by the higher intensity of the diffraction peak at this temperature. It was evident from the AFM micrographs that the shape of the grains does not change with increasing substrate temperature. XPS spectra reveal the presence of ZrN phase. Laser Raman revealed a definite correlation of the obtained results with the compositional analysis.

References

[1]   W. J. Chou, C. H. Sun, and G. P. Yu, Mater. Chem. Phys. **82**, 228 (2003).
[2]   A. Mitsuo, T. Mori, Y. Setswhar, S. Miyake, and T. Aizawa, Nncl. Inst. Meth. B **206**, 366 (2003).
[3]   A. Rizzo, M. A. Signore, L. Mirenghi, and D. Dimaio, Thin Solid Films **515**, 1486 (2006).
[4]   H. Jimenez, E. Restrepo, and A. Devia, Surf. Coat. Tech. **201**, 1594 (2006).
[5]   H. J.Ramos and N. B.Valmoria, Vacuum **73**, 549 (2004).
[6]   Wen-Jun Chou, Chun-Hsing Sun, Ge-Ping Yu, and Jia-Hong Huang, Mater. Chem. Phys. **82**, 228 (2003).
[7]   Chuan-Pu Liu and Heng-Ghieh Yang, Thin Solid Films **444**, 111 (2003).
[8]   A. I. Ivanovskii, N. I. Medvedeva, and S. V. Okatov, Inorg. Mater. **37**, 459 (2001).

[9]   J. A.Sue and H. H.Troue, Surf. Coat. Technol. **39/40**, 421 (1989).
[10] M. B. Lee, M. Kawasaki, M. Yoshimtot, M. Kumagai, and H. Koinuma, Jpn. J. Appl. Plys. **33**, 6308 (1994).
[11] C. H. Ma, J. H. Huang, and H. Chen, Surf. Coat. Technol. **133/134**, 289 (2000).
[12] D. Wu, Z. Zhang, W. Fu, X. Fan, and H. Guo, Appl. Phys. A **64**, 593 (1997).
[13] L. Pichon, A. Straboni, T. Girardeau, and M. Drouet, J. Appl. Phys. **87**, 925 (2000).
[14] V. N. Zhitomirsky, I. Grimberg, R. L. Boxman, N. A. Travitzky, S. Goldsmith, and B. Z. Weiss, Surf. Coat Technol. **94/95**, 207 (1997).
[15] K. Salmenoja and A. S. Korhonen, Vacuum **36**, 33 (1986).
[16] J. A. Sue and H. H. Troue, U.S Patent application **905**, 510 (1986).
[17] Chuan-Pu Liu and Heng-Ghieh Yang, Mat. Chem. Phys. **86**, 370 (2004).
[18] O. Knacke, O. Kubaschewski, and K. Hesselmann, Thermochemical properties of inorganic substance II, 2nd edition (Springer-Verlag, Berlin, 1991), pp. 2103-2409.
[19] J. H. Huang, C. Y. Hsu, S. S. Chen, and G. P. Yu, Mater. Chem. Phys. **77**, 14 (2003).
[20] D. J. Kim, Y. M. Yu, S. H. Eorn, T. H. Kim, C. S. Go, and Y. D. Choi, Mater. Chem. Phys. **92**, 274 (2005).
[21] R. W. Hoffman, Surf. Interf. Anal. **3**, 62 (1981).
[22] D. K. Lee, J. J. Lee, and J. Joo, Surf. Coat. Technol. **174-175**, 1234 (2003).
[23] D. Wu, Z. Zhang,W. Fu, X. Fan, and H. Guo, Appl. Phys. A **64**, 593 (1997).
[24] C. P. Constable, J. Yarwood, and W. D. Munz, Surf. Coat. Tech. **116-117**, 155 (1999).
[25] A. Cassinese, M. Iavarone, R. Vaglio, M. Grimsditch, and S. Uran, Phys. Rev. B **62**, 5699 (2000).
[26] W. C. Oliver and G. M. Phar, J. Mater. Res. **7**, 1564 (1992).
[27] P. H. Maryhofer, A. Horling, L. Karlson, J. Sjolen, T. Larsson, C. Mitterer, and L. Hultman, Appl. Phys. Lett **83**, 2049 (2003).